Islamic Azad University
Mashhad Branch

# Structural analyses of fault planes using fault slickenlines and calcite e-twins data from the Dasht-e-Arjan graben, SW Iran

**Zahra Kamali[1], Jafar Rahnamarad[*2], Khalil Sarkarinejhad[1]**

*1. Department of Geology, College of Sciences, University of Shiraz, Shiraz, Iran*
*2. Department of Geology, Zahedan Branch, Islamic Azad University, Zahedan, Iran*

Received 28 October 2016; accepted 13 April 2017

## Abstract

Dasht-e-Arjan is a northeast trending graben located 65 km west of Shiraz. It was formed along active segments of the Korrehbas fault, perpendicularly to the Shahnesh in and Salamati anticlines. Oriented sampling from bordering fault planes and striations was carried out to evaluate the relative amounts of paleostress/strain needed to form the graben. Measurements of e-twins and c-axis of calcite properties on XY and XZ planes, using five universal stages in a polarizing optical microscope, showed the presence of type I and II calcites. Because the calcite e-twins and fault striations register the last deformation phase, measurements of calcite e-twins show the plane strain K=1 in the last graben deformation phase. The inversion method, applied for the analysis of fault striation data, showed a plane stress ellipse ($\varphi$=1), ($\sigma_1$=$\sigma_2$), and a plane strain ellipse ($r_0$=1). The mean orientation of the sub-vertical maximum principal-stress ($\sigma_1$) was N23°.70°E, and the mean orientation of minimum principal-stress ($\sigma_3$) was S58°.26°E. Based on the analysis of twinned calcite crystals, the mean direction of the determined compression and tension were S55°E ± 9.−32° and N35°E±11.−72°, respectively. Using multiple inversion methods, and based on the investigation of fault striation data, we can expect two stress phases. The paleostress phase, acting as a tensional regime, caused the formation of SW trending faults, while the recent phase caused the formation of new fractures within the study area. Based on field and laboratory analyses, it is suggested that a tension tectonic regime is dominant in the studied graben.

***Keywords:*** *Inversion method; tensional regime; paleostress; striation; polarizing.*

## 1. Introduction

The Zagros folded belt gradually leads northeast to a thrust area (Zagros thrust system) and develops a long, narrow, active fault zone 10–70 kilometres wide, located between the high pressure–low temperature Sanandaj- Sirjan metamorphic belt and parallel to the Zagros fold belt (Burg and Chen1984; Berberian 1995; Regard et al. 2004) (Fig 1). This part is called the inner Zagros because it is the innermost part of the Zagros zone (Berberian and King 1981; Authemayou et al. 2006). Deformation in the eastern Zagros (Fars zone) includes shortening, parallel to the convergence, and elongation, which can be attributed to the activation of Korehbas, Sabzpushan, Kazerun, and Sarvestan faults (Leturmy et al. 2010; Talebian and Jackson 2004;Rahnama-Rad et al. 2009). Paleostress reconstruction methods used mechanical interpretations of rock structures and microstructures, such as fault striations, to deduce the tectonic evolution of a region. In this regard, researchers compared the magnitude and orientation of in situ-stress, and earthquake focal mechanisms, to estimate the direction of stress and paleostress (Rahnama- Rad et al. 2008; Viola et al. 2013; Lacombe 2007).

---

*Corresponding author.
*E-mail address (es):* jrahnama2003@gmail.com

Continental platforms are keys to tectonic evolution reconstruction. Different methods are applied to measure paleostress tensors, such as mathematical methods based on the inversion of fault slip data (Michael 1984). The analysis of compressional and tensional structures (joints and stylolites) hasbeen recently used, in addition to other methods (Angelier 1984). Fault slip data inversion is applied to analyse field-based fault slip and fault striation data. The main problem in using inversion data is the determination of local stress tensor on multiple faults, with respect to the slip direction. Here the main assumption is that any fault slip, which is marked by a specific fault striation, has a direction of a unit tensor. Fault striation data were collected within six stations along the Oligo-Miocene limestone Asmari Formation, for the determination of compressional and tensional paleostress direction by fault slip inversion. Over the past years, determination of paleostress has been conducted using various methods by several researchers. Graphical methods (Arthaud 1969; Angelier and Mechler1977; and Lisle 1987) and numerical techniques (Carey and Brunier1974; Etchecopar et al. 1981; Armijo et al. 1982; Angelier 1984, 1989; and Michael 1984) have been used.


Fig 1. Major structural units of Zagros fold-thrust belt.

In the graphical method, for each individual fault, the maximum and minimum stresses ($\sigma_1$ and $\sigma_3$) are confined to the fields bounded by the fault plane, and by an imaginary plane being normal to the slip line on the fault surface (Shan et al. 2009). Based on a numerical analysis of fault- slip data sets, the stress field reconstruction of deformed rocks is a key to understanding tectonic events in the studied areas (Fry 1999; Yamaji 2000; Shan et al. 2004a and 2004b; Kernstockova and Melichar 2009). Calcite twinning is one of the most important temperature independent deformation mechanisms, and it has low critical shear-stress. Unlike most sliding systems, twining occur at low temperature and low confining pressure. In this process, twinning cannot solely lead to high strain because one slip system acts independently. However, at the grain scale, it leads to discontinuous shearing and results in considerable strain at grain boundaries. In microscopic studies, calcite is used as a natural micro-gauge in the calculation of compressional and extensional tensors, and it is a useful tool for computation of governing stresses within the brittle deformation phases' region. Most minerals have potential twinning planes within their structures. These twinning structures can occur during both recrystallization and deformation (Twiss and Moores 1992). Twin gliding is the process where an e-twin forms parallel to the twinning plane during simple shear. In this study, oriented samples (including calcite crystals) were separated to prepare thin sections along XY and XZ planes. Then, using an optical microscope equipped with five universal stages, calcite crystals e-twins and c-axis were measured. To analyse the data, Castries software was used to calculate five parameters: c-axis orientation, e-twins pole, orientation after compression, orientation after tension and the angle between e-twin poles and c-axis orientation. In this study, our data was collected along the Oligo-Miocene Asmari Formation (Fig 2).

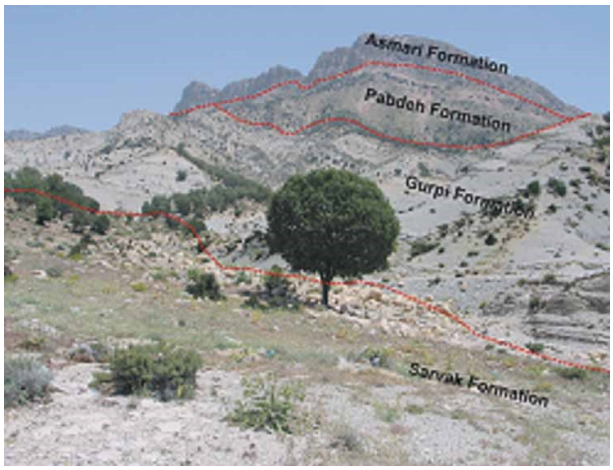


Fig 2. Stratigraphic formations in the North limb of the Shahneshin anticline (observer facing NW).

## 2. Geological setting

The study area was located in the folded Zagros, which is a part of the Zagros fold-thrust belt (Sarkarinejad and Azizi 2008, Sarkarinejad and Ganbarian 2014). Dezful embayment divides the Zagros fold-thrust belt into Fars and Lorestan provinces. Structural and topographical changes divided the belt into two NE−SW trend domains (Agard et al. 2011). The first domain is the simply folded belt (SFB), which extends by Persian Gulf with almost a hundred metres of regular folds

(Falcon 1974; Sepehr and Cosgrove 2004; Mouthereau et al. 2006), associated with some blind faults. The second domain is High Zagros (HZ), which has a higher elevation than the folded belt (Fig 1). The Dasht-e-Arjan Pond is one of the valuable ecosystems of the Fars province, with about 1000 hectares (Fig 3). The water level elevation from the pond floor varies between 1 and 4 metres in depressions and sinkholes, particularly in dry seasons. This pond is situated65km northwest Shiraz. Due to the existence of Asmari, Pabdeh and Gurpi and Sarvak formations, limestone is the most exposed rock unit in the area (Figs 2 and 3). The region contains about 100 $km^2$ ponds and 32.5 $km^2$plains and mountainous areas (Eskandari 1973), and it is mainly covered with about 10 km thick sedimentary layers (Kamali et al. 2013).

Dasht-e- Arjan is a graben formed between two faults, the eastern Arjan and western Arjan faults, with strike and dip N55E/70NW and N45E/ 78SE, respectively (Fig 4). Their normal faulting, with sinistral strike-slip component, was deduced from displacement. The conjunction of narrow bays and the fault blocks movement direction was deduced using rake of striations on fault planes. The average inclination angle on east and west Arjan faults are 87° and 56°, respectively (Fig 5). Despite the activity of the two normal faults, there is no stratigraphic tilting within the study area. One of the visible signatures of the normal faults is a stratigraphic hiatus, due to the downward movement of the hanging wall. The west Arjan fault scarp has a 75° dip angle with about 150m vertical displacement, while the east Arjan fault scarp has a 79° dip angle and about 500 m vertical displacement (Fig 6). The elevation difference between the two graben sides can be attributed to the Asmari (limestone) Formation, which crops out throughout the study area. In addition to these faults, there are other structures including Shahneshin (Dali) anticline, Bayal anticline, Salamati anticline and Domasbi syncline (Fig 4). Because of the frequent activity of fault blocks, exposure of structures such as fault slickensides, fault striations and fault breccia, was observed (Fig 7).

## 3. Research Methodology

In this research, oriented samples containing calcite twins from fault slickensides were collected for preparation of thin sections in XY and XZ planes (Fig 8). Then, using an optical microscope equipped with five universal stages, calcite crystals e-twins and c-axes were measured. To analyse the data, the CALC Stress software was used.

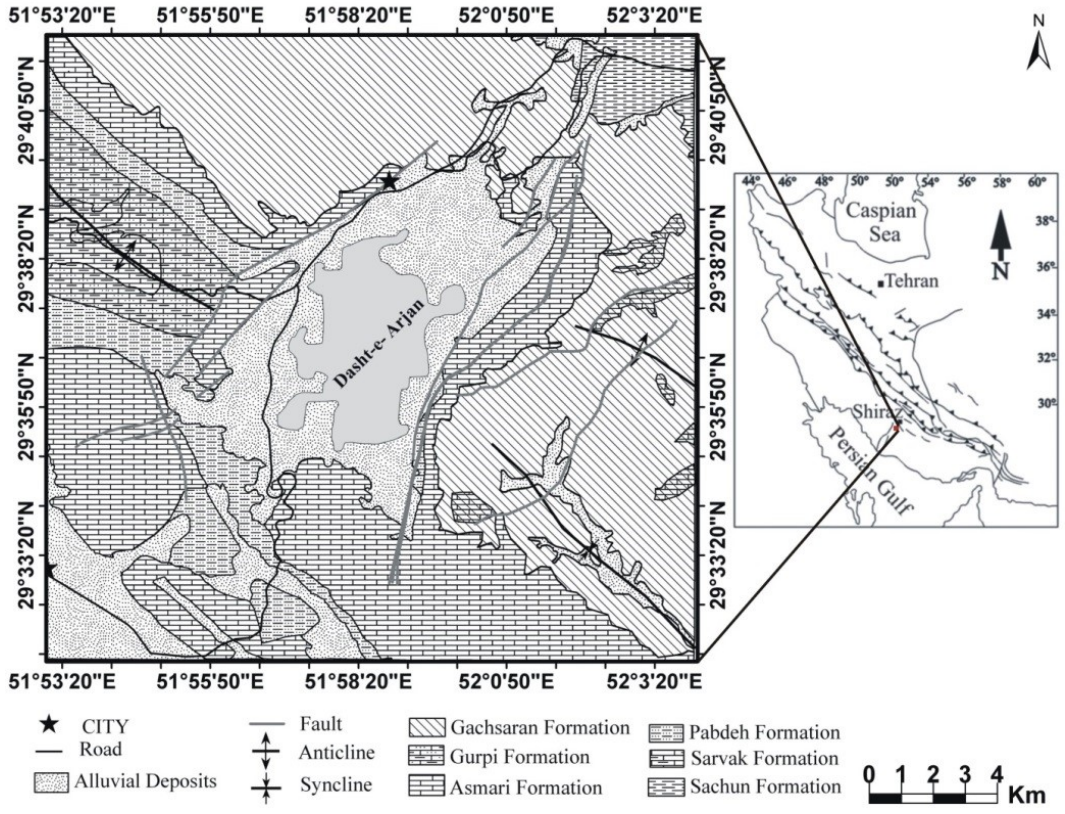


Fig 3. Schematic geological map of Dasht-e-Arjan (adapted from the Kazerun geological maps 1:100000, Fakhari 1979).

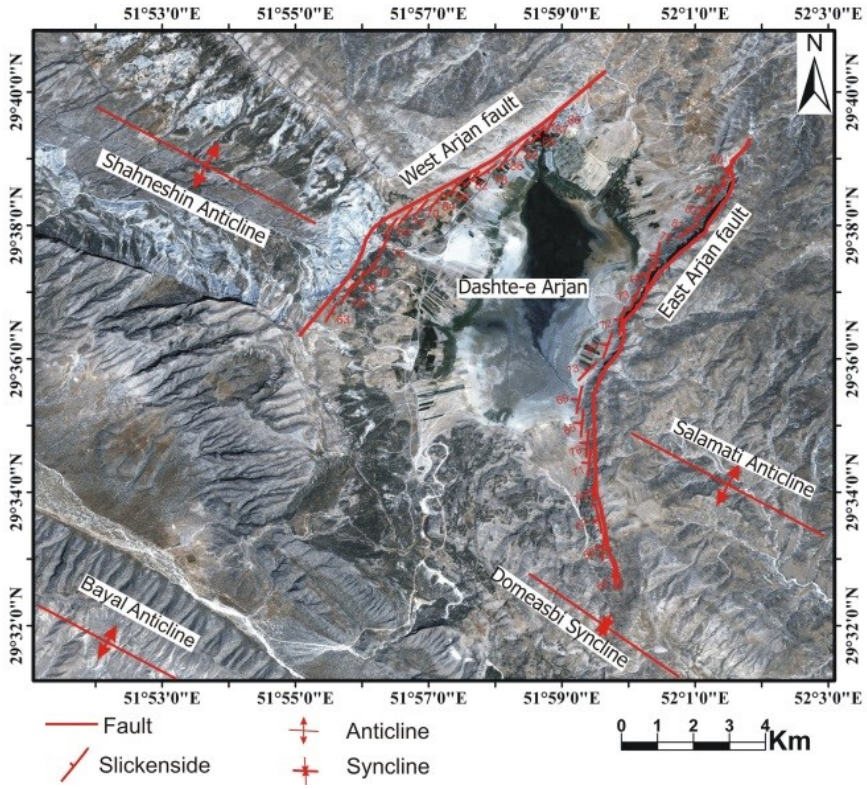


Fig 4. Structural map of Dasht-e-Arjan, as a graben formed between two faults, the eastern and western Arjan faults, on the Spot image.


Fig 5. (a)The average inclination angle on east Arjan (b) and west Arjan faults.

The software calculated five parameters: c-axis orientation, e-twins pole, orientation after compression, orientation after tension and the angle between piles of e-twin and c-axis orientation. For the determination of main strain axes relative magnitude, the Spheri-Stat software was used. For the determination of paleostress direction and separation of tectonics phases, using the inversion method, fault striation data was collected in six stations ($S_1$=19, $S_2$=25, $S_3$=21, $S_4$=28, $S_5$=25, $S_6$=15) along the Oligo-Miocene limestone Asmari Formation. The 'Faultkin5winbeta' and 'T-Tecto 3' software were used for the determination of the compression and tension axes andtheseparation of tectonics phases, respectively.


Fig 6. (a) The west Arjan fault scarp has a 75° dip angle with about 150m vertical displacement (b), where the east Arjan fault scarp has a 79° dip angle and about 500 m vertical displacement.

Fig 7. West Arjan fault wall with slickensides, striations and breccia that were formed because of the operation of fault (observer facing NW).

The calcite crystal oriented samples were carefully collected from fault striations, and thin sections in XY and XZ directions were prepared from them. The twinned calcitese- twin poles and c-axis were measured by a polarized microscope equipped with five universal stages. The obtained values were analysed by the CALC-Stress software, which has a five-column output table with c-axis orientation, e-twin pole, compression orientation, tension orientation and the angle between e-twin pole and c-axis orientation. Then, separate stereonet projections were prepared for nine sampling stations (S1=71, S2=92, S3=78, S4=71, S5=71, S6= 91, S7=74, S8=80, and S9=73),whose positions are marked in the Dasht-e-Arjan geological map. A further collection of fault striation data, along the Oligo-Miocene Asmari Formation (Fig 9), was conducted to calculate the main stress relative magnitude and strain axes and to determine the strain ellipsoid shape using the Gauss method. The T-Tecto 3.0 software was used to analyse these data and to extract information on stress and strain state.

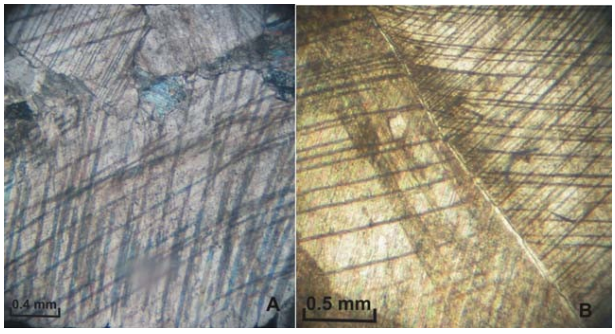


Fig 8. Microscopic samples prepared for calcite e-twins: (a) Presence of thick type I twins in a thin section and (b) Presence of thick and thin calcite type II e-twins.


Fig 9. Fault striation data collected from West Arjan slickenside (observer facing NW).

## 4. Discussion

Strain is one of the important characteristics of a deformed rock (Ramsay 1967). To measure strain values, the primary and final shapes of a material that has undergone a deformation process are required. Calcite crystal, which has a measurable final shape, is suitable for this purpose. This method can be used in the calculation of internal strain if a deformed rock has suitable calcite crystals to measure the optical axes. Using the U-Stage method it is possible to determine the orientation of host crystals, e-twin pole, the amount and thickness of e-twins and the thickness of a crystal perpendicular to the e-twin plane (Groshong 1972).

### 4.1 Calcite e-twins Analysis

There are some noteworthy points about the strain of brittle zones. First, due to the region's brittle deformation and rock unit segmentation and consequently, the presence of segments with different alignments, different force distribution and stress components were locally observed. Second, all thin sections showed elongation, as they were collected from growing calcite fibres of fault slickensides. Elongation in other sections occurred because of crystal growth in open spaces during fault creeping, and it was not related to the strain. Based on previous classifications (Burkhard 1993; Groshong et al. 1984; Rowe and Rutter 1990; Evans and Dunne 1991;Ferrill 1991; Ferrill et al. 2004), the thin twins type I is formed at shallow depths, at 170 to 200°C, with less than 1 µm thickness, while type II is formed at200 to 300°C, with more than 1 µm thickness. On the other hand, types III and IV are probably formed at higher depths and temperature, so they reach the ground surface with some rotation (Fig 10) (Spanos et al., 2015). These type I and II calcite e-twins were reliable markers for the measurements. It was observed that all samples collected from the study area contained only calcite e-twins type I and II, indicating their formation at shallow depths and low temperature.

The diagram of Flinn (1962) is plotted using two magnitude ratios of three eigenvectors of an orthogonal diagram. Based on the equation $S_1+S_2+S_3=1$, in this diagram there was no elimination of data because only two numbers of these three parameters are mutually independent (Fig 11). The majority of points obtained from the analysis of calcite crystals were placed on Flinn diagram K=1 line (Fig 12), indicating an anisotropic distribution. This distribution was due to formation of calcite crystals in constant volume coaxial plane strain conditions. The anisotropic distribution of these points shows a tri-axial strain, indicating calcite crystals were formed under plane strain condition. The C parameter, which is the ability of data for preferred orientation, was obtained by the equation $C= \ln (S_1/S_3)$. The mean C parameter obtained from the analysis of elongated calcite crystals was about 1.3228. With respect to the obtained average of point distribution and dispersion in the Flinn diagram, it can be stated the calcite crystals have a random distribution, since their main concentration was around the diagram's origin. Table 1 shows the eigenvalues obtained from the twinned calcite crystals analysis.

### 4.2 Stress and strain pattern Analysis

Some errors occurred during data collection, resulting in dispersion of local stress pattern. Thus, in practice, it was necessary to search for the best fitting fault striation data of a specific tectonic event. To recognize and analyse the paleostress axes arrangement, direct field sampling was conducted during the surveying process. All of our data collection stations were in Oligo-Miocene Asmari Formation. In this work, 123 geological data were collected from fault slip planes and fault striations. After collecting fault plane properties, T-Tecto 3.0 software was used to calculate the study area relative amounts of prevailing stress and strain. The mean inclinations on eastern and western Arjan fault slickensides are 87° and 56°, respectively. As the first

step, the fault plane specifications were collected, and the slip trend was determined using the fault striations measures. Analyses of the fault striation data suggested a spatial arrangement of $\sigma_1$ NNE, a nearly vertical plunge for $\sigma_3$ and SE and an almost horizontal plunge for $\sigma_2$ and SW. Spatial stress configurations were N23°E70°,S58°E26° and S34°W10° for $\sigma_1$, $\sigma_3$ and $\sigma_2$, respectively (Figs 13 and 14). The mean direction of the determined compression and tension from twinned calcite crystals analysis were S55°E±9, 32° and N35°E±11, 72°, respectively. Figures 15 and 16 represent each station's values.

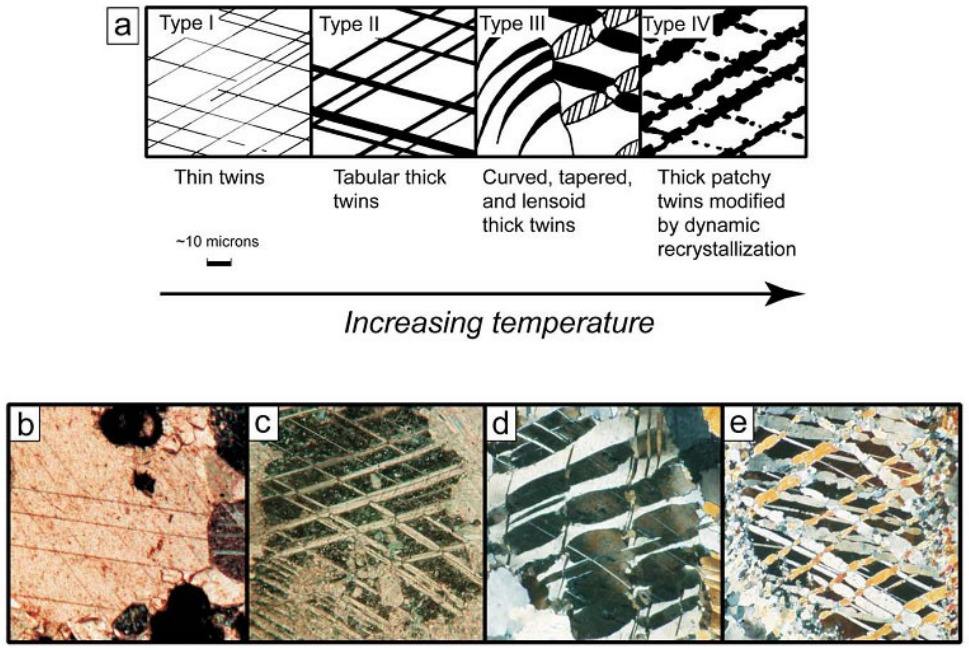


Fig 10. (a) Schematic illustration of temperature influence on the formation of calcite twins: (b) type I; (c) type II; (d) type III and (e) type IV (Burkhard 1993).

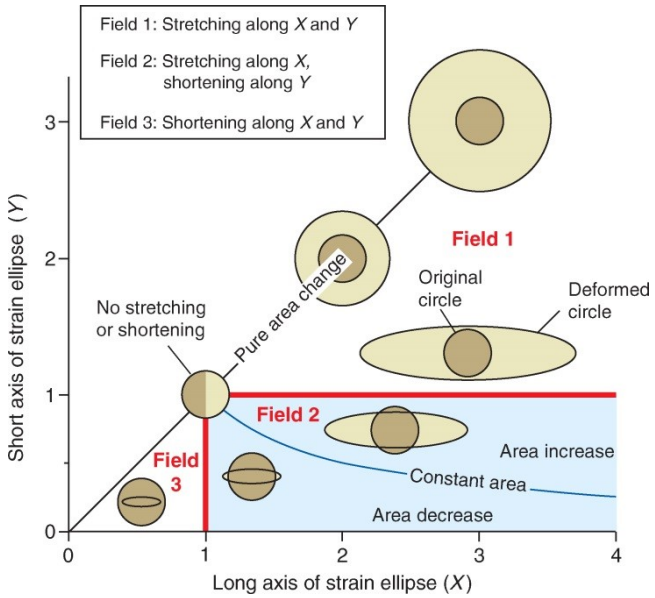


Fig 11. Modified Flinn diagram, by Ramsay (1967).

Table 1. The distribution of points on the stereo net, based on Woodcock (1977).

| Station | N | $S_1$ | $S_2$ | $S_3$ | K | C | Ln ($s_2/s_3$) | Ln ($s_1/s_2$) |
|---|---|---|---|---|---|---|---|---|
| 1 | 80 | 0.5431 | 0.3019 | 0.8081 | 0.8801 | 1.2539 | 0.6420 | 0.5097 |
| 2 | 72 | 0.4991 | 0.2032 | 0.0850 | 1.5118 | 1.9901 | 0.6464 | 0.2246 |
| 3 | 82 | 0.4682 | 0.377 | 0.1535 | 0.2453 | 1.1133 | 0.5202 | 0.7787 |
| 4 | 79 | 0.5342 | 0.3059 | 0.1620 | 0.5940 | 1.2049 | 0.6473 | 0.5288 |
| 5 | 130 | 0.4709 | 0.4036 | 0.1255 | 0.1324 | 1.3220 | 0.4372 | 0.4328 |
| 6 | 83 | 0.4470 | 0.3469 | 0.2061 | 0.4873 | 1.2742 | 0.6739 | 0.7605 |
| 7 | 69 | 0.5082 | 0.2875 | 0.2043 | 0.9114 | 1.6667 | 0.7848 | 0.5430 |
| 8 | 94 | 0.4963 | 0.3783 | 0.1159 | 0.2041 | 1.4549 | 0.4393 | 0.7395 |
| 9 | 127 | 0.4380 | 0.3793 | 0.1425 | 0.1369 | 1.1591 | 0.5017 | 0.8527 |

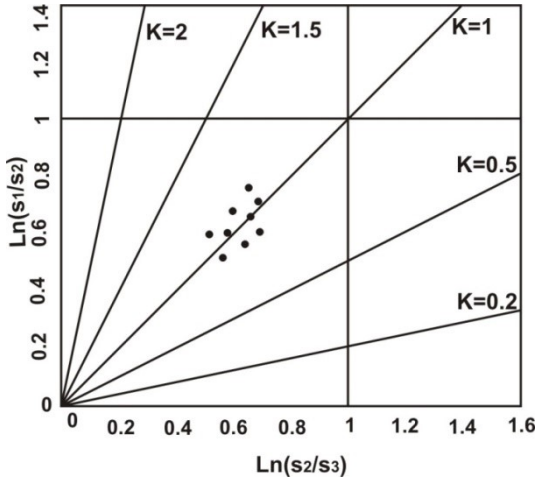


Fig 12. Normalized eigenvalues of S1, S2 and S3 in thin sections of the study area, plotted on a Flinn diagram (Ramsay 1967).

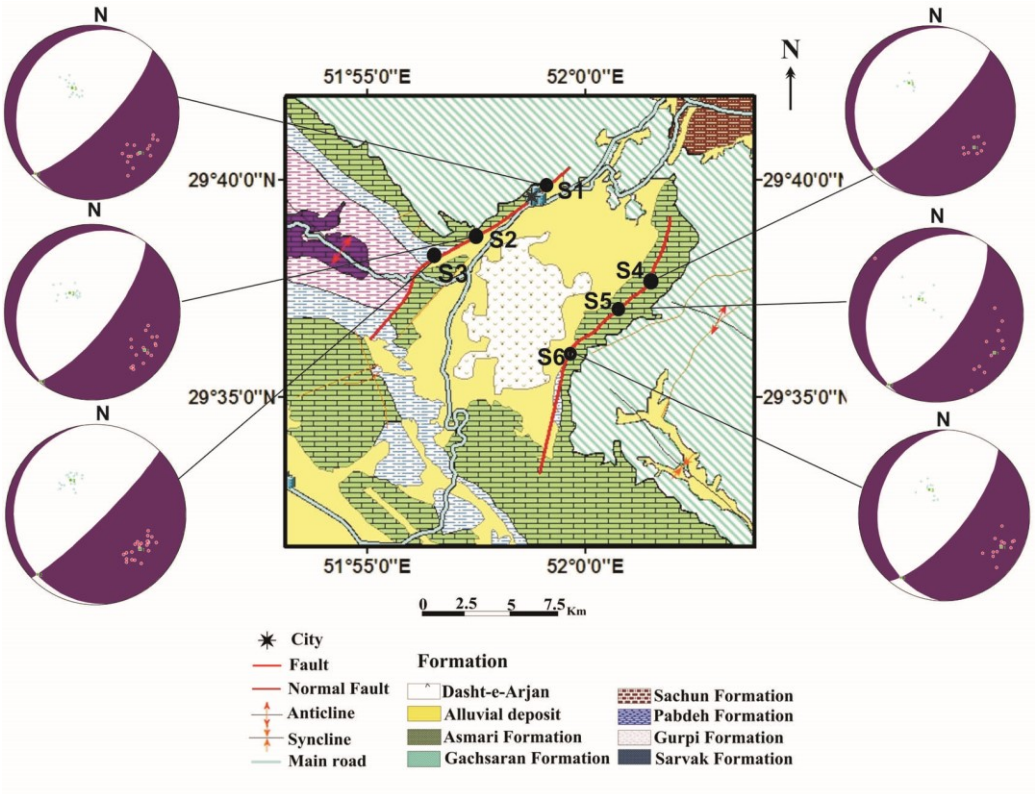


Fig 13. patial arrangement of the stress axes (compression and tension direction) with focal mechanisms of the earthquakes of the Dasht-e-Arjan.

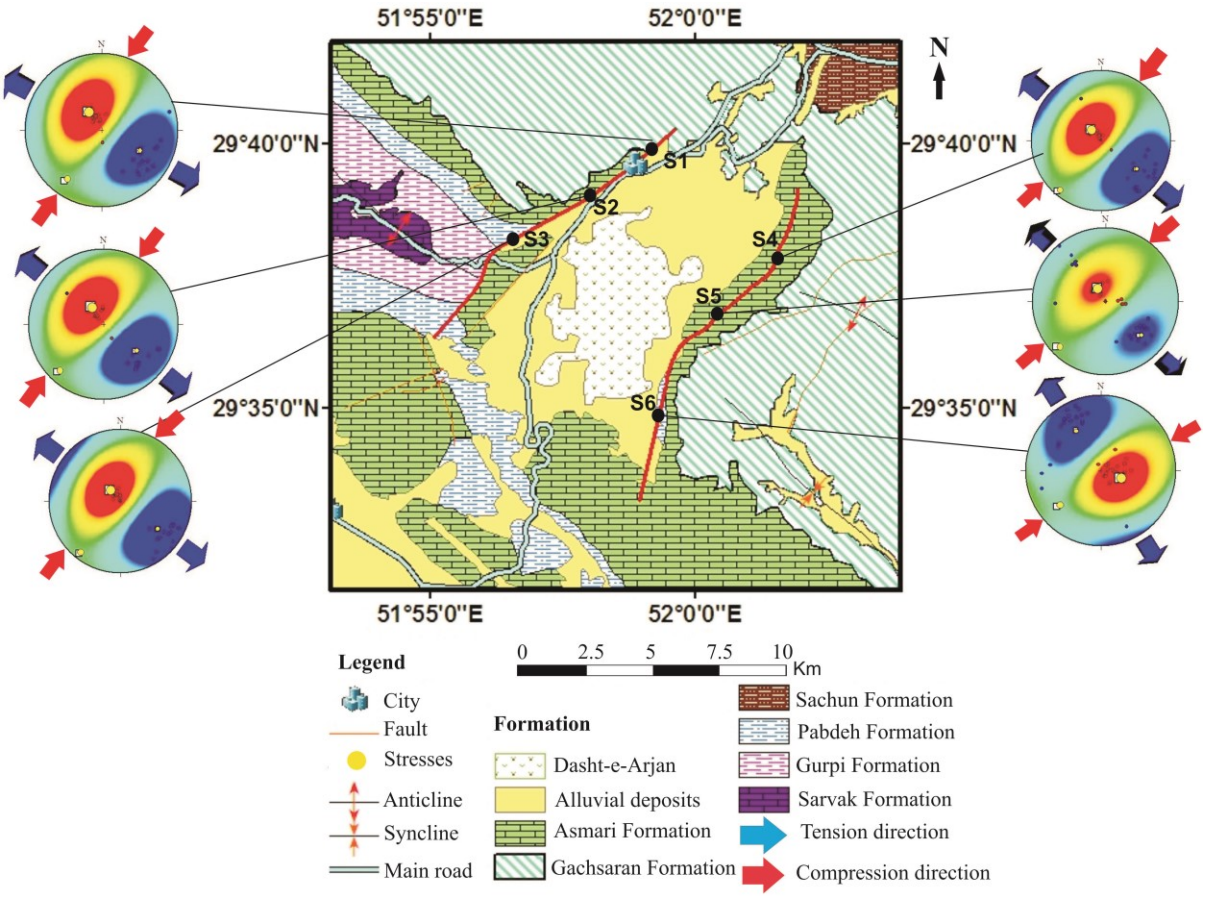


Fig 14. Stereo net projections obtained from analysis of the fault striation data in the Arjan graben, using the inversion method of fault slip data.

Although for most conditions, it is not possible to determine the main stresses absolute values the relative magnitude of stress and strain we can be estimated eventually, using fault slip data. For this purpose, the R parameter ($R= (\sigma_2-\sigma_3) /(\sigma_1-\sigma_3)$) was used to determine the tectonic regimes, where usually $0<R<1$. Conditions $R=0$, $R=1$ and $R=0.5$ indicate the radial, axial extension and general extension, respectively. Figure 17 illustrates the Mohr circles plotted with fault slip data and their former tectonic regime. Accordingly, three main tectonic regimes were differentiated, with reference to the vertical principal stress: $\sigma_1$vertical -extensional tectonic regime,$\sigma_2$ vertical-wrench regime (strike slip) and $\sigma_3$vertical- compression regime. The relative magnitudes of principal stresses vary continuously between these three end-member tectonic regimes, and the transition from one regime to another is fundamentally due to permutation of one of the horizontal principal stress axes with the vertical one. Each tectonic regime may vary continuously from radial to axial, depending on the relative magnitudes of the intermediate principal stresses, $\sigma_2$, with respect to the extreme principal stresses, $\sigma_1$ and $\sigma_3$. The R-value obtained in the study area was1, indicating axial extension (Figs 17 and 18). The normal faults with strike-slip or oblique-slip components are formed within transtension conditions (Twiss and Unruh 1998).

Fossen (2012) applied the equation $\varphi = (\sigma_2-\sigma_3) /(\sigma_1-\sigma_3)$ for the determination of strain ellipsoid shape. In this equation, $\varphi$ parameter is commonly in the range of $0<\varphi<1$. The $\varphi=0$ indicates an oblique strain ellipsoid where $\sigma_2=\sigma_3$ and compression conditions are dominant. On the other hand, the $\varphi=1$ shows an oblate strain ellipsoid with $\sigma_1=\sigma_2$, which is related to tension (Fig 19). Figure 20 illustrates the principal stress differences, where $\sigma_1$-$\sigma_2$is plotted against $\sigma_2$-$\sigma_3$and brings out the shapes of plotted-stress tensors. On this picture, stress states with the same value are plotted on straight lines radiating from the origin, although their position along the lines depends on the differential stress value, $d= \sigma_1-\sigma_3$, and $\varphi$ is the stress shape ratio (Ramsey and Lisle 2000).

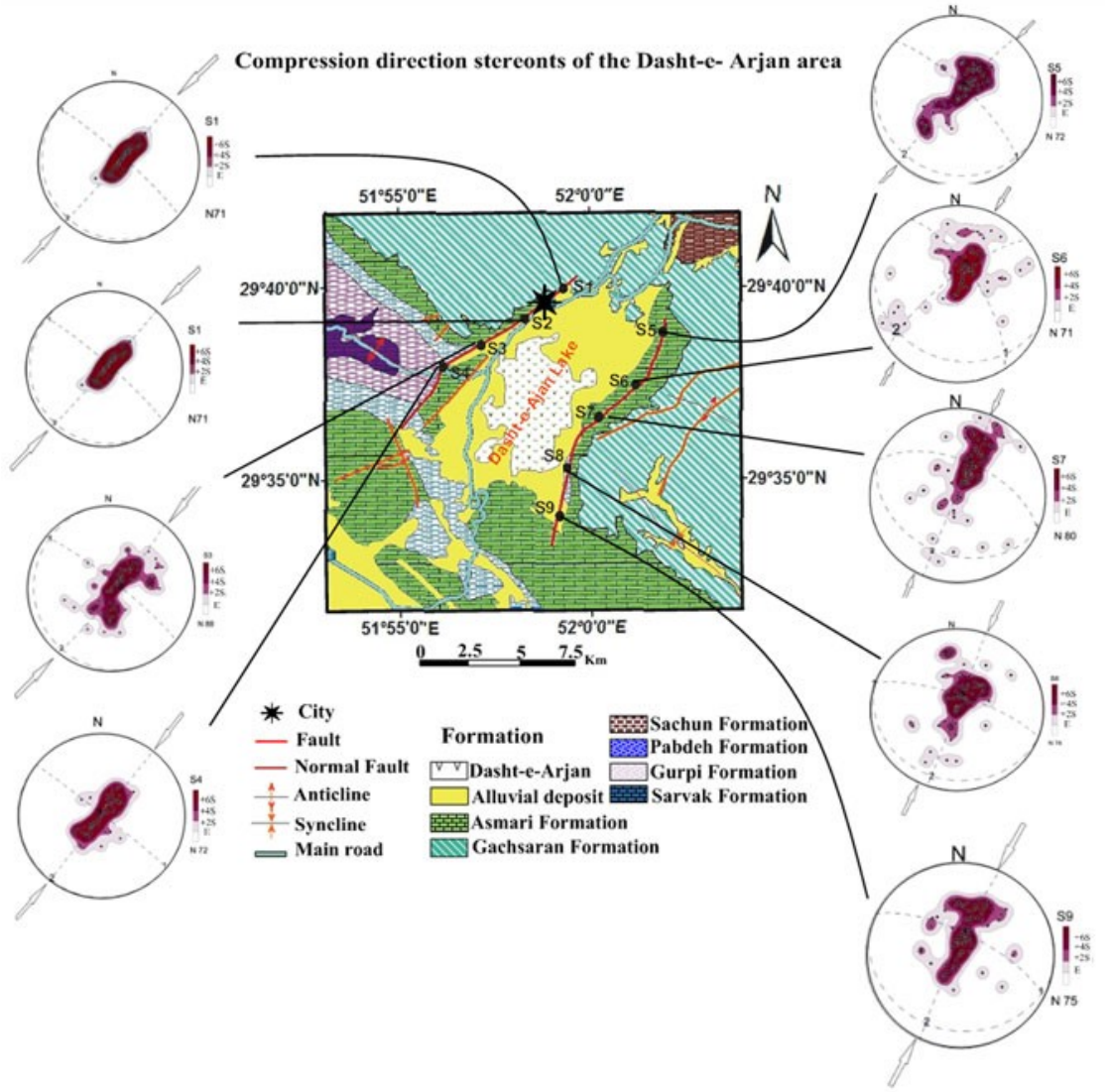


Fig 15. Compression directions of Dasht-e-Arjan graben sampling stations.

The obtained φ parameter is 1′ (φ=1), implying the presence of oblate strain ellipsoid and tension. In addition, the strain ellipsoid shape can be estimated based on fault slip data analysis and the ratio φ= $(\sigma_1-\sigma_2)$ / $(\sigma_1-\sigma_3)$ (Lisle and Leyshon 2004). Based on the fault slip data analysis, it can be stated that tension was the prevailing mechanism in the study area.

Shape of strain ellipsoid can be obtained using ther$_0$ parameter ($r_0$= $(E_2-E_3)$/ $(E_1-E_3)$), where $E_1$, $E_2$ and $E_3$ are eigenvalues of moment tensors (Bingham 1964), obtained from the primary data processing conducted by Fault Kin 5 WinBeta software. Different values of $r_0$=1, $r_0$=0 and $r_0$=0.5 indicate the oblate strain ellipsoid, constructional strain ellipsoid and plane strain ellipsoid, respectively (Federico et al. 2010). Taking into account these expressions and the collected fault slip data, the study area $r_0$was1, indicating oblate strain ellipsoid (Fig 21, Table 2).

Table 2. Relative values of principal strains.

| $E_1$ | $E_2$ | $E_3$ | $r_0$ |
|---|---|---|---|
| 0.62 | -0.31 | -0.31 | 1 |

To determine the inverse paleostress based on fault striation data, the T-Tecto 3.0 software was used, and the results yielded two different deformation phases. In this stress analysis method, it was assumed that the fault striations show maximum shear-stress direction (Zalohar and Vrabec 2007). Then, by inverting these phenomena, it is possible to obtain the stresses caused by formation of fault planes and fault striations. Phase1 and 2 deformations showed newer strains, and the youngest deformation was related to the second phase (Fig 22).

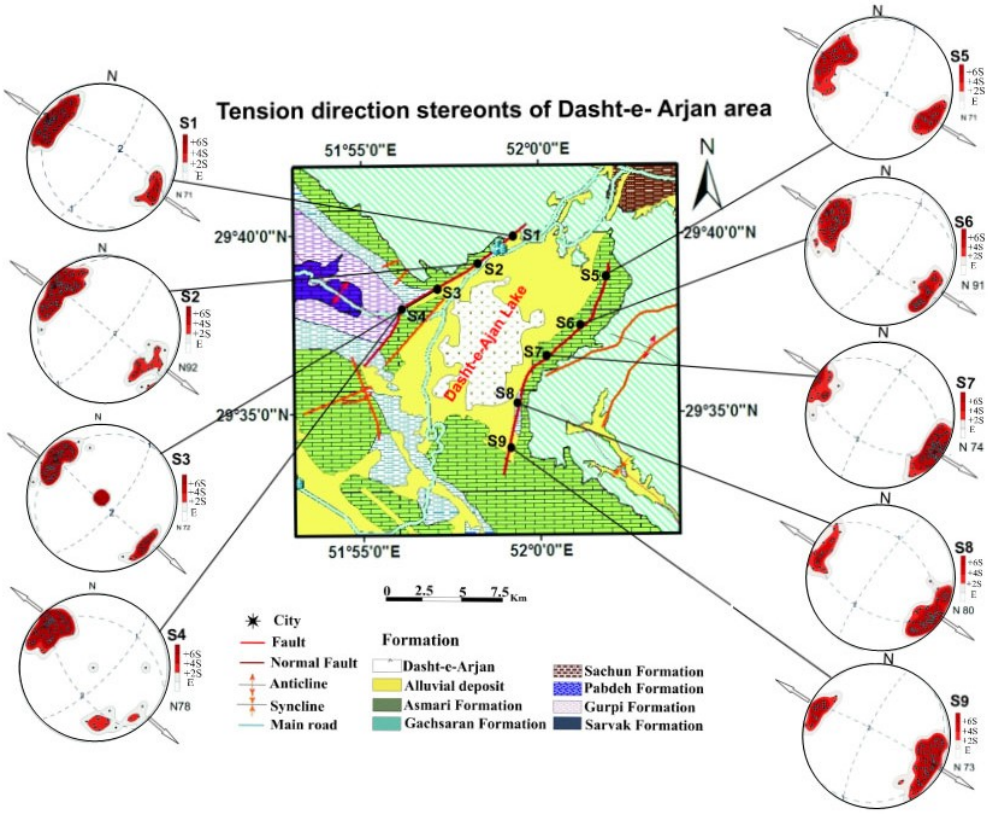


Fig 16. Tension directions of Dasht-e-Arjan graben sampling stations.

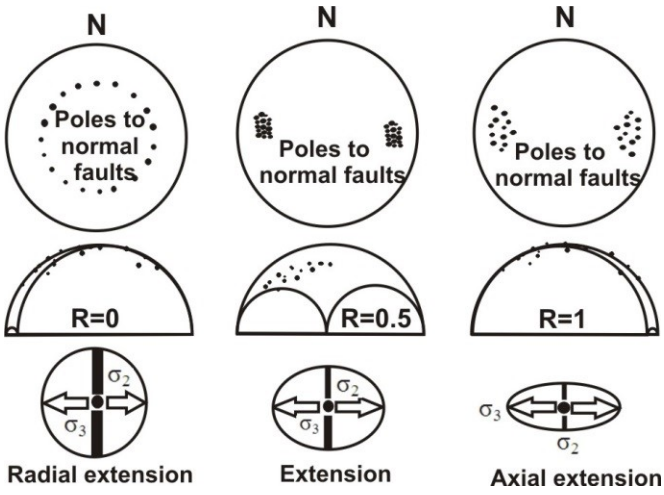


Fig 17. Tectonic regime and Mohr circles plotted with fault slip data (Twiss and Unruh 1998).

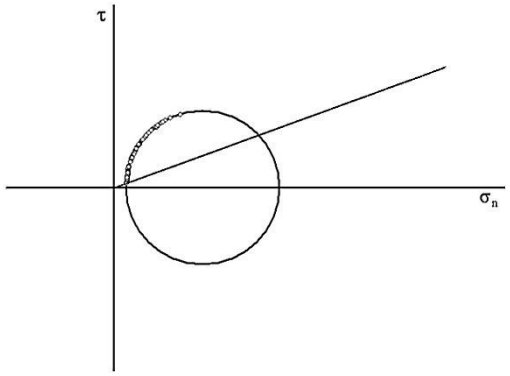


Fig 18. The Mohr circle plotted with fault striation data of the study area.

### 4.3 Inversion Analysis

Based on investigation of fractures and fault striations formed within the study area, and using a multiple inversion method with the T-Tecto 3.0 software, two stress phases can be expected in the study area. In the first tectonic deformation phase, $\sigma_2$ and $\sigma_3$werehorizontal while, $\sigma_1$ was vertical (Ramsay 1967; Ramsay and Lisle 2000). In the second deformation phase, $\sigma_3$wasnearly horizontal, $\sigma_2$washorizontal and σ was vertical. With respect to orientation of stress directions, these two phases showed normal faulting. This analytical method showed the area experienced two different deformation phases and a tensional tectonic regime. The first identified tectonic phase was caused by the formation of fractures and main faults (with NE–SW trends) and joints that were filled and cemented in the study area (Fig 23). It seems that this stress phase formed the study area overall structure. The second phase, the youngest governing stress phase, was caused by formation of recent fractures.

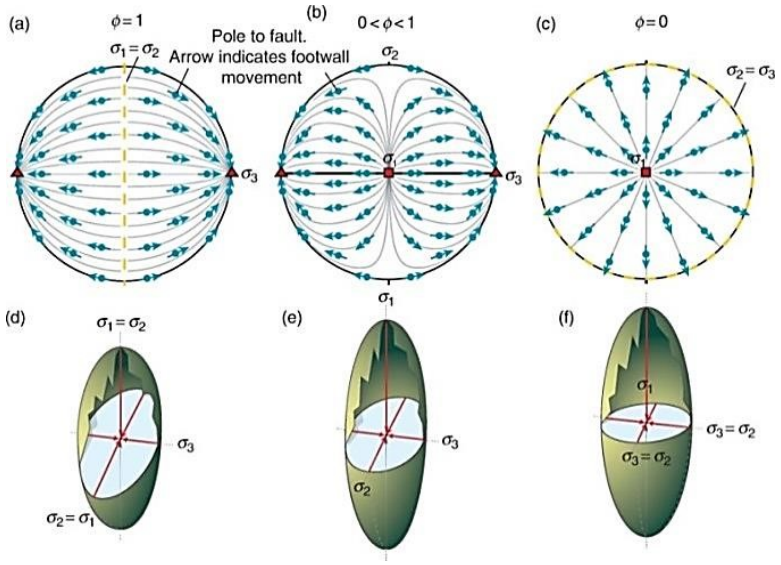


Fig 19. Strain ellipsoid shapes interpreted from the values of the $\varphi = (\sigma_2-\sigma_3) / (\sigma_1-\sigma_3)$ formula (Twiss and Moores 2007).

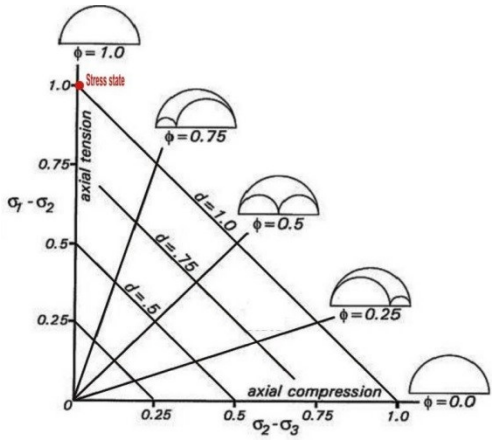


Fig 20. Stress tensor diagram of φ parameter derived from T-Tecto 3.0, for the entire study area.

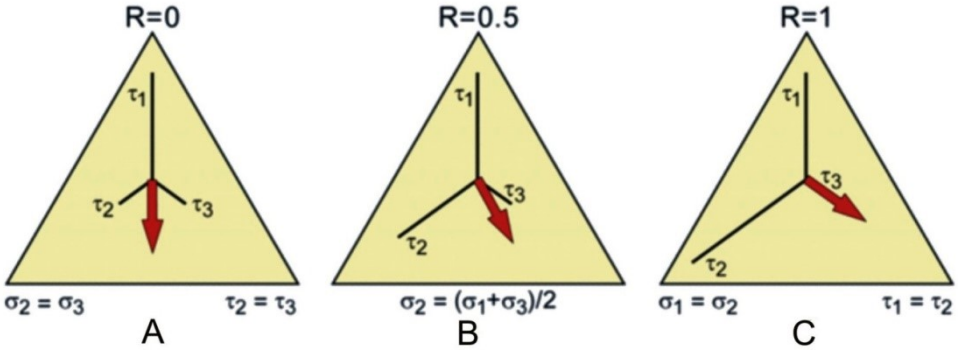


Fig 21. Various positions of the shear plane with respect to τ1, $\tau_2$ and $\tau_3$ stresses. (a) slip vector parallel to $\tau_1$, (b) slip vector between $\tau_1$ and $\tau_3$, (c) slip vector parallel to $\tau_3$ (Twiss and Unruh 1998).

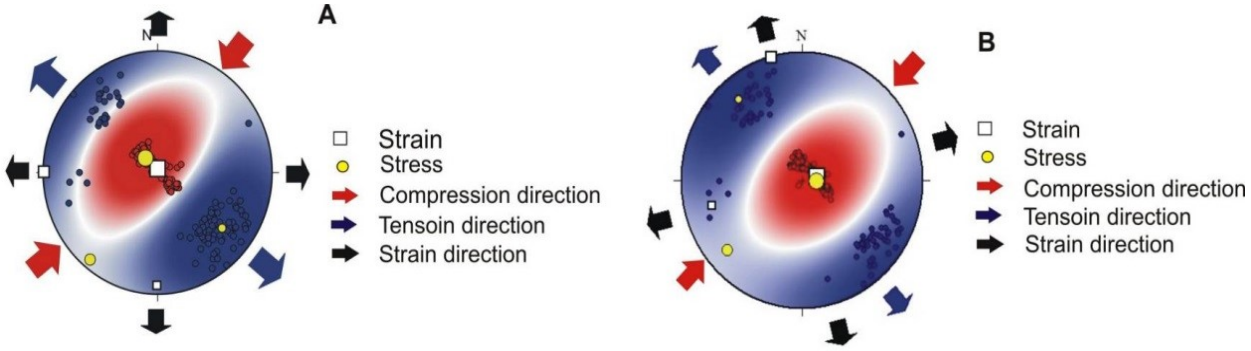


Fig 22. First and second tectonic phases (a and b) derived from the inversion method, for the study area.

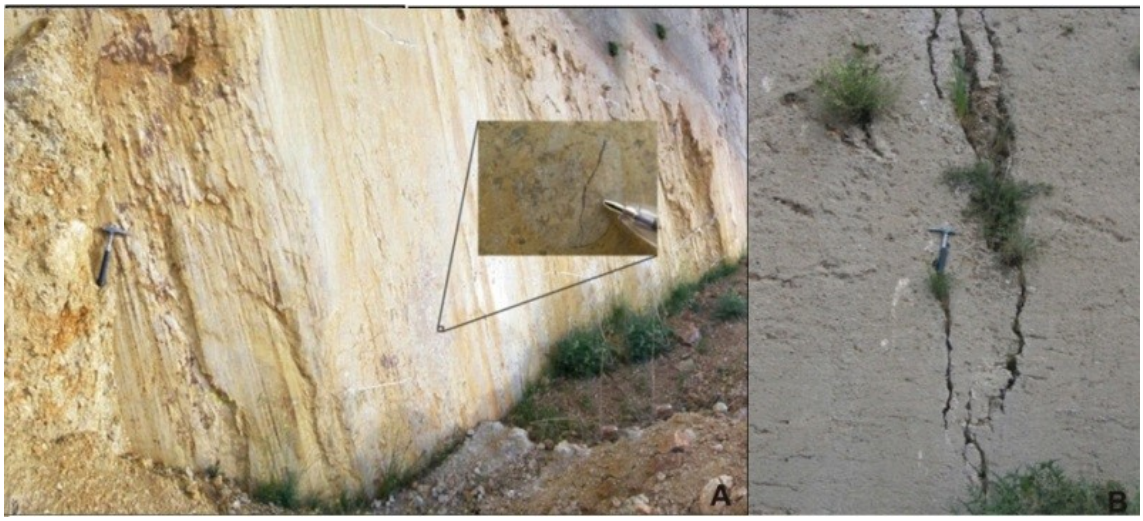


Fig 23. (a) First deformation phase which indicates fractures, major faults, fault joints, filling, and cement in the western Arjan (the observer facing northwest; and (b) Second phase causing young joints (the observer's the northeast).

## 5. Conclusion

Paleostress analysis on the basis of the fault slip inversion method was performed from striations, or slickenlines, data collected from two faults planes. It showed that the orientation of the maximum principal-stress ($\sigma_1$) of the graben isN23°E72°and minimum principal-stress ($\sigma_3$) is S58°E26°. Microscopic examinations of oriented thin sections (XY- and XZ-planes) indicated that they consisted of type I and Π calcite e-twins. Measurements of the e-twin and c-axis were carried out using an optical polarising microscope equipped with five universal stages, to determine the orientations of 'Compression' (P) and 'Tension' (T) axes. The mean orientation of the sub-vertical maximum principal-stress ($\sigma_1$) is N35°E ± 11.72°, and the mean orientation of minimum principal-stress ($\sigma_3$) is S55°E ± 9.32°.

The results of studies on twinned calcite crystals showed that most data had k=1, indicating the tendency of data for anisotropic distribution. This distribution is due to formation of calcite crystals in constant volume coaxial plane strain conditions. In addition, calcite crystals had a random distribution, with respect to the presence of type I and type II calcite e-twins in the study area. Thus, it can be suggested that they were formed at shallow depth and low temperature conditions. The results of fault striation data analysis, tectonic regime and shape of the Mohr circle of the study area indicated the presence of axial extension and extensional tectonic regime. The stress ellipsoid shape, φ =1,showedtension and plane stress ellipsoid, while the stress shape ratio φ =1 indicated axial tension. Besides, the shape of the strain ellipsoid with $r_0$=1showedoblate strain ellipsoid for fault striation data. In this work, two tectonic phases were identified within the study area. The first one is caused by the formation of fractures and main faults (with NE–SW trends) and joints filled and cemented. It seems that this stress phase had the greatest impact on structure formation within the study area. The second phase, as the youngest governing stress phase, was caused by formation of recent fractures, where the related tensional stress was aligned in NW-SE direction. The two identified phases of tension and compression directions showed a relative 20° clockwise rotation. All investigation conducted in this work were in the Oligo-Miocene Asmari Formation because of its exposure and considerable thickness in the study area. The obtained results are related to the last stage of deformation and operation of the graben faults, because twinned calcite crystals and fault striations recorded the last deformation stage. The results indicated operation of the tensional tectonic regime that is well consistent with Anderson theory of normal faulting (Twiss and Moores 2007).

## Acknowledgement

The authors thank the research council of Shiraz University for providing the part of the research facilities.

## References

Agard P, Omradi J, Jolivet L, et al. (2011) Zagros orogeny: a subduction-dominated process, *Geology Magazine* 148 (5-6): 692-725.

Angelier J (1984) Tectonic analyses of fault slip data sets. *Journal of Geophysical Research* 89 (No.B7): 5835–5848.

Angelier J (1989) From orientation to magnitudes in paleostress determinations using fault slip data, *Journal of Structural Geology* 11: 37–50.

Angelier J, Mechler P (1977) Sur une méthode graphique derecherche des contraintes principales égalment utilisable en tectoniqueet en seismologie: La method desdièdres droits, *Bulletin Société Géologique de France* 19: 1309–1318.

Armijo R, Carey E, Cisternas A (1982) The inverse problem in microtectonics and the separation of tectonic phases, *Tectonophysics* 82: 145–160.Arthaud F (1969) Méthode de détermination graphique des directions de raccourcissement, d'allongement et intermédiaire d'une population de failles, *Bulletin de la Société Géologique de France* 11 (5): 729–737.

Authemayou C, Chardon DE, Bellier O et al. (2006) Late Cenozoic partitioning of oblique plate convergence in the Zagros Fold-and-Thrust belt (Iran), *Tectonics* TC3002: 25.

Berberian M (1995) Master blind thrust fault hidden under the Zagros folds: Active basement tectonics and surface morphotectonics, *Tectonophysics* 241: 193-224. Berberian M, King GCP (1981) Toward a paleo-geography and tectonic evolution of Iran, *Canadian Journal of Earth Sciences* 18 (2): 210-265.

Bingham C (1964) Distributions on a sphere and the projective plane. PhD thesis 93 p, Yale University, New Haven.

Burg JP, Chen GM (1984) Tectonics and structural zonation of southern Tibet, China, *Nature* 311: 219 – 223.

Burkhard M (1993) Calcite twins, their geometry, appearance and significance as stress-strain markers and indicators of tectonic regime: a review, *Journal of Structural Geology* 15: 351-368.

Carey E, Brunier B (1974) Analyse the orique et nume rique d'une mode le me menique é le mentaire appliqué a l'etude d'une population de failles. C.R. Acad, *Society Paris. Ser.* D 279: 891–894.

Eskandari M (1973) Investigation of regional hydrology Dasht- e- Arjan (Gulf). A report by the Southern Regional Water Authority (Gulf).

Etchecopar A, Visseur G, Daignieres M (1981) An inverse problem in microtectonics for the determination of stress tensors from fault striation analysis, *Journal of Structural Geology* 3: 51–65.

Evans M, Dunne W (1991) Strain factorization and partitioning in the North Mountain thrust sheet, central Appalachians, USA, *Journal of Structural Geology* 13: 21–36.

Fakhari M (1979) Geological maps Kazeroon 1/100000. National Iranian Oil Company.

Falcon N (1974) Southern Iran: Zagros Mountains in Mesozoic-Cenozoic Orogenic Belts: Data from organic studies (Ed. A M Spencer), *Geological Society of London Special Publication* 4: 199–211.

Federico L, Crispini L, Capponi G (2010) Fault-slip analysis and transpressional tectonics: A study of Paleozoic structures in northern Victoria Land, Antarctica, *Journal of Structural Geology* 32 (5): 667-684.

Ferrill D A (1991) Calcite twin widths and intensities as metamorphic indicators in natural, low-temperature deformation of limestone, *Journal of Structural Geology* 13: 667–675.

Ferrill D A, Morris P, Evans M, et al. (2004) Calcite twin morphology: a low-temperature deformation geothermometer, *Journal of Structural Geology* 26: 1521–1529.

Flinn D (1962) On folding during three-dimensional progressive deformation, *Quarterly Journal of the Geological Society* 118: 385-434.

Fossen H (2012) Structural Geology. Cambridge University Press, New York. 549.

Fry N (1999) Striated faults: visual appreciation of their constraint on possible paleostress tensors, *Journal of Structural Geology* 21: 7-21.

Groshong RH Jr (1972) Strain calculated from twinning in calcite, *Geological Society of American Bulletin* 83: 2025–2038.

Groshong RH Jr, Teufel LW, Gasteiger C (1984) Precision and accuracy of the calcite strain-gauge technique, *Geological Society of American Bulletin* 95: 357–363.

Kamali Z, Sarkarinejad K, Rahnamarad J (2013) Structural analyses of the Dasht-e-Arjan Graben: using remote sensing techniques and slikenlines, *Journal of Applied Geology* (In Persish, Abstract in English) 9(2): 135-148.

Kernstockova M, Melichar R (2009) Numerical paleostress analysis – the limits of automation, Trabajos de Geología, *Universidad de Oviedo* 29: 399-403.

Lacombe O (2007) Comparison of paleostress magnitudes from calcite twins with contemporary stress magnitudes and frictional sliding criterion the continental crust: Mechanical implications, *Journal of Structural Geology* 29: 86-99.

Leturmy P, Molinaro M, Frizon de Lamotte D (2010) Structure, timing and morphological signature of hidden reverse basement faults in the Fars Arc of the Zagros (Iran). In Tectonic and Stratigraphic Evolution of Zagros and Makran during the Mesozoic–Cenozoic. In: Leturmy P, Robin C (eds), *Geological Society of London, Special Publication* 330: 121–38.

Lisle R J (1987) Principal stress orientations from faults: an additional constraint, *Annales Tectonicae* 1 (2): 155–158.

Lisle R J, Leyshon P R (2004) Stereographic Projection Techniques for Geologists and Civil Engineers. Cambridge University Press 124.

Michael A J (1984) Determination of stress from slip data, faults, and folds, *Journal Geophysical Research* 89: 11517-11526.

Mouthereau F, Lacombe O, Meyer B (2006) The Zagros folded belt (Fars, Iran): constraints from topography and critical wedge modeling, *Geophysical Journal International* 165: 336–56.

Rahnama-Rad J, Derakhshani R, Farhoudi G, et al. (2008) Basement faults und salt plug emplacement in the Arabian Platform in southern Iran, *Journal of Applied Science* 8 (18):3235-3241.

Rahnama-Rad J, Farhoudi G, Ghorbani H, et al. (2009) Pierced salt domes in the Persian Gulf and in the Zagros mountain ranges in southern Iran and their relationship to hydrocarbon and basement tectonics, *Iranian Journal of Earth Sciences* 1: 57-72

Ramsay JG (1967) Folding and fracturing of rocks. McGraw-Hill, New York, 568.

Ramsay JG, Lisle RJ (2000) Applications of continuum mechanics in structural geology. The techniques of modern structural geology 3: 11 pages, Academic Press, London.

Regard V, Bellier O, Thomas JC, et al. (2004) Accommodation of Arabia-Eurasia convergence in the Zagros-Makran transfer zone, SE Iran: A transition between collision and subduction through a young deforming system, *Tectonics* 23 (4): TC 4007.

Rowe K, Rutter E (1990) Paleostress estimation using calcite twinning: experimental calibration and application to nature, *Journal of Structural Geology* 12 (1): 1–17.

Sarkarinejad K, Azizi A (2008) Slip partitioning and inclined dextral transpression along the Zagros Thrust System, Iran, *Journal of Structural Geology* 30 (1): 116-136.

Sarkarinejad K, Ghanbarian M A (2014) The Zagros hinterland fold-and thrust belt in-sequence thrusting, *Journal of Asian Earth Sciences* 85: 66-79.

Sepehr M, Cosgrove JW (2004) Structural framework of the Zagros Fold-Thrust Belt, Iran, *Marine and Petroleum Geology* 21: 829–843.

Shan Y, Li Z, Lin G (2004a) A stress inversion procedure for automatic recognition of polyphase fault/slip data sets, *Journal of Structural Geology* 26: 919-925.

Shan Y, Lin G, Li Z (2004b) An inverse method to determine the optimal stress from imperfect fault data, *Tectonophysics* 387: 205-215.

Shan Y, Tian Y, Xiao W (2009) Incorporating imaginary faults in graphical stress methods, *Journal of Structural Geology* 31: 366–368.

Spanos D, Xypolias P and Koukouvelas I (2015) Vorticity analysis in calcite taconite's: An example from the Attico-Cycladic massif (Attica, Greece), *Journal of Structural Geology* 80: 120-132.

Talebian M, Jackson J (2004) A reappraisal of earthquake focal mechanisms and active shortening in the Zagros mountains of Iran. *Geophysical Journal International* 156: 506-526.

Twiss RJ, Moores EM (2007) Structural Geology. 2nd edition. New York: HW Freeman and Company.

Twiss RJ, Unruh JR (1998) Analysis of fault slip inversions: Do they constrain stress or strain rate?, *Journal of Geophysical Research* 103: 12202- 12222.

Viola G, Zwingmann H, Mattila J, et al. (2013) K-Ar illite age constraints on the Proterozoic formation and reactivation history of a brittle fault in Fennoscandia. *Terra Nova* 25 (3): 236–244.

Woodcock N H (1977) Specification of fabric shapes using an eigenvalues method, *Geological Society of America Bulletin* 88: 1231-1236.

Yamaji A (2000) The multiple inverse method: a new technique to separate stresses from heterogeneous fault-slip data, *Journal of Structural Geology* 22 (4): 441–452.

Zalohar J, Vrabec M (2007) Paleostress analysis of heterogeneous fault-slip data, The Gauss method, *Journal of Structural Geology* 29: 1798-1810.